



# Treatment of secondary brain injury by perturbing postsynaptic density protein-95-NMDA receptor interaction after intracerebral hemorrhage in rats

Zhifeng Wang<sup>1,\*</sup>, Zhouqing Chen<sup>1,\*</sup>, Junjie Yang<sup>2</sup>, Ziyang Yang<sup>2</sup>, Jia Yin<sup>1</sup>, Xiaochun Duan<sup>1</sup>, Haitao Shen<sup>1</sup>, Haiying Li<sup>1</sup>, Zhong Wang<sup>1</sup> and Gang Chen<sup>1</sup> 

## Abstract

Postsynaptic density protein-95 (PSD95) plays important roles in the formation, differentiation, remodeling, and maturation of neuronal synapses. This study is to estimate the potential role of PSD95 in cognitive dysfunction and synaptic injury following intracerebral hemorrhage (ICH). The interaction between PSD95 and NMDA receptor subunit NR2B-neurotransmitter nitric oxide synthase (nNOS) could form a signal protein complex mediating excitatory signaling. Besides NR2B-nNOS, PSD95 also can bind to neurexin-1–neuroligin-1 to form a complex and participates in maintaining synaptic function. In this study, we found that there were an increase in the formation of PSD95-NR2B-nNOS complex and a decrease in the formation of neurexin-1–neuroligin-1-PSD95 complex after ICH, and this was accompanied by increased neuronal death and degeneration, and behavior dysfunction. PSD95 inhibitor Tat-NR2B9c effectively inhibited the interaction between PSD95 and NR2B-nNOS, and promoted the formation of neurexin-1–neuroligin-1-PSD95 complex. In addition, Tat-NR2B9c treatment significantly reduced neuronal death and degeneration and matrix metalloproteinase 9 activity, alleviated inflammatory response and neurobehavioral disorders, and improved the cognitive and learning ability of ICH rats. Inhibition of the formation of PSD95-NR2B-nNOS complex can rescue secondary brain injury and behavioral cognitive impairment after ICH. PSD95 is expected to be a target for improving the prognosis of patients with ICH.

## Keywords

Cognitive dysfunction, intracerebral hemorrhage, postsynaptic density protein-95, rats, secondary brain injury

Received 2 July 2017; Revised 6 February 2018; Accepted 10 February 2018

## Introduction

Intracerebral hemorrhage (ICH) is a worldwide public health problem; high mortality and morbidity rates are associated with hemorrhagic stroke.<sup>1,2</sup> In addition to the mechanical effects including cerebrovascular rupture and hematoma caused by primary brain injury, secondary brain injury (SBI) has been proven to contribute to neurological deterioration after ICH.<sup>3,4</sup> Although various treatments have been tried, only 20% of ICH patients are currently able to resume functional life within 6 months after clinical treatment.<sup>3,5</sup> SBI is a very important factor affecting the poor prognosis of patients after ICH.<sup>6,7</sup> Therefore, the prevention of SBI after ICH is very important.<sup>8</sup>

<sup>1</sup>Department of Neurosurgery & Brain and Nerve Research Laboratory, The First Affiliated Hospital of Soochow University, Suzhou, China

<sup>2</sup>Institute for Cardiovascular Science & Department of Cardiovascular Surgery of the First Affiliated Hospital, Soochow University, Suzhou, China

\*These authors contributed equally to this work.

### Corresponding authors:

Gang Chen, Department of Neurosurgery & Brain and Nerve Research Laboratory, The First Affiliated Hospital of Soochow University, 188 Shizi Street, Suzhou 215006, China.

Email: nju\_neurosurgery@163.com

Wang Zhong, Department of Neurosurgery & Brain and Nerve Research Laboratory, The first Affiliated Hospital of Soochow University, 188 Shizi Street, Suzhou 215006, China.

Email: 13280008348@163.com

SBI is often accompanied by neuronal damage and apoptosis after ICH. This process is often due to hematoma compression and synaptic damage induced by blood toxic components, while a large number of neurons can't function normally.<sup>9,10</sup> Chronic hypertension leads to cerebrovascular dysfunctions that may increase injury and increase synaptic response.<sup>11,12</sup> The recovery of neurological function after ICH is realized via brain structural and functional reorganization, which is defined as brain plasticity. And brain plasticity is partly due to the increase in the number of synapses and the enhancement of synaptic function.<sup>9,13</sup> The increase in the number of synapses and the enhancement of function can increase the association between neurons, inhibit the initiation of apoptosis, and enhance the activity of peripheral neurons in cerebral hemorrhage.<sup>14</sup> Thus, the study of neurological synaptic molecules during SBI may provide a new therapeutic target for patients with ICH.<sup>8,10,14</sup>

The postsynaptic density protein (PSD) family has a number of protein members and acts as a scaffold to provide neurotransmitter receptor assembly, the occurrence of adhesion molecules, and signal transduction.<sup>15</sup> Among the family members, PSD95 contains a GK region (region homologous to yeast guanylate kinase), a SH3 (Src-homology-3) domain or WW motif (two conserved tryptophan residues), and 3 PDZ domains (domain first discovered in PSD95/Dlg/ZO1 proteins).<sup>15,16</sup> In the excitatory synapses, PSD95 binds to the NMDA receptor subunit NR2B and neurotransmitter nitric oxide synthase (nNOS) through the second PDZ domain to form a signal protein complex that plays a key role in mediating the conduction of excitatory signaling and maintaining the excitatory balance of synapses.<sup>15,17</sup> Matrix metalloproteinases (MMPs) have been shown to participate in the pathogenesis of ICH.<sup>18,19</sup> Neuronal nitric oxide synthase (nNOS) promotes the production of nitric oxide, which subsequently induced S-nitrosylation and activation of MMP-9 and finally induced neuronal apoptosis.<sup>20</sup> Neurexin-1 and neuroligin-1 separately locate at the presynaptic membrane and postsynaptic membrane, and both of them can be connected into a complex across the presynaptic and posterior membrane.<sup>21</sup> In addition to NR2B and nNOS, PSD95 can bind to neuroligin-1 through its third PDZ domain and indirectly link to neurexin-1 to form a complex and participate in synaptogenesis, differentiation, remodeling, maturation, and the balance of synaptic function.<sup>21,22</sup> PSD95 plays an important role in the repair of PSD region injury. The PSD region is important for synaptic integration and recovery of neurological function. However, the potential role of PSD95 in ICH-induced SBI and how PSD95 switches between NR2B-nNOS and neurexin-1 and neuroligin-1 have not been reported.

In this study, we investigated the relationship between PSD95 and NR2B-nNOS, the relationship between PSD95 and neurexin-1 and neuroligin-1 in a rat ICH model generated by collagenase injection, and the effect of PSD95 inhibitor Tat-NR2B9c on ICH-induced SBI. The Morris water maze test was performed to assess neurobehavioral function after synaptic remodeling in rats after ICH.

## Materials and methods

### Experimental animals

All male Sprague Dawley (SD) mice about 8 weeks old and weighing 250–300 g were provided by the Shanghai Experimental Animal Center of the Chinese Academy of Sciences. All management procedures were approved by the Suzhou University Animal Protection Committee and were conducted in accordance with the National Institutes of Health's guidelines on the care and use of animals. All animal research data are written according to ARRIVE (Animal Research: Reporting of in vivo Experiments) guidelines. Sample sizes were determined by power analysis during the animal ethics dossier application. The rats were housed at relative humidity (40%) and constant temperature (23°C) under a regular light/dark schedule. Food and water were available ad libitum. For grouping animals, rats were randomly numbered, and Stat Trek's Random Number Generator was used for selecting random samples. All the capture and quantitative analysis were performed by observers who were blind to the experimental group.

### Establishment of collagenase ICH model in rats

The SD rat collagenase ICH model was established as described previously.<sup>23</sup> Briefly, the rats were anesthetized and fixed in a brain stereotactic instrument (ZH-Lanxing B type stereotactic frame, Anhui Zhenghua Biological Equipment Co. Ltd., Anhui, China). According to the rat head stereotactic anatomical map,<sup>24</sup> we determined the drilling position (coronal and sagittal midline at the intersection of 0.2 mm, sagittal right 3.5 mm) for the right basal ganglia open window diameter of about 2 mm, and 1  $\mu$ L of 0.23U collagenase VII in physiological saline was slowly injected into the basal ganglia with a 10- $\mu$ L microinjector (Hamilton). The collagenase injection rate was 0.2  $\mu$ L/min for 5 min. The micro-syringe was stagnated for 10 min and then was slowly pulled out after injection. The sham operation group received basal ganglia injection of equal volume of physiological saline solution. During the establishment of the model, the heart rate, blood pressure, and body temperature were

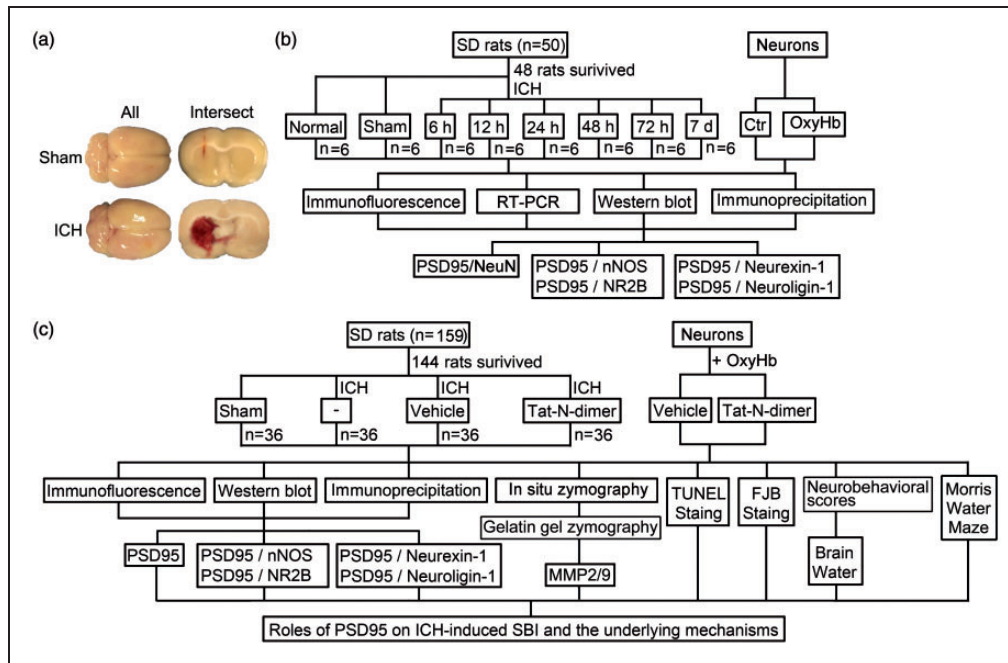


**Figure 1.** Intracerebral hemorrhage model and experimental design. (a) Whole brain and the largest coronal section of hematoma. (b) Time course of PSD95 expression in brain tissue after ICH. The interaction between PSD95 and NR2B-nNOS and neurexin–neuroigin was observed after ICH. (c) Roles of PSD95 on ICH-induced secondary brain injury and the underlying mechanisms. PSD95: postsynaptic density protein-95; ICH: intracerebral hemorrhage; nNOS: neurotransmitter nitric oxide synthase.

monitored in real time, and the rectal temperature was maintained at 37.5°C. According to Berderson et al.,<sup>25</sup> the assessment method is divided into four levels. A schematic illustration of the ICH model is shown in Figure 1(a).

#### Establishment of autologous blood ICH model in rats

A autologous blood ICH model in rats was performed as previously reported.<sup>8</sup> Briefly, 100 µL of autologous blood was collected from the heart using a 100 µL microsyringe (Hamilton Company, Nevada, USA) and slowly inserted into the subdural space 5.5 mm in depth to reach the basal ganglia at an injection rate of 10 µL/min.

#### Cell culture and establishment of *in vitro* ICH model

Primary rat cortical neurons were isolated and cultured in accordance with a previous experimental study.<sup>26</sup> Briefly, cortical neurons were isolated from 16- to 18-day gestational age embryos and treated with Trypsin-EDTA solution for 5 min at 37°C. Dissociated neurons were plated onto plates (Corning, USA) precoated with 0.1 mg/ml poly-D-lysine (Sigma, USA), cultured in Neurobasal-A medium supplemented with 2% B-27 and 0.5 mM GlutaMAX™-I (all from Invitrogen, Grand Island, NY), and maintained at 37°C under

humidified conditions and 5% CO<sub>2</sub>. Half of the medium was exchanged for fresh medium every 2 days for approximately 2 weeks before exposure to treatment.

#### Experimental grouping

The *in vivo* experiments were divided into two parts. In experiment 1, 48 rats (50 rats were used, 48 survived after the surgery) were randomly assigned into eight groups and each group had 6 rats: normal group, sham group, and 6, 12, 24, 48 and 72 h, 7 days after ICH. The first step was to investigate the changes of PSD95 expression in brain tissue at different time points after ICH. Our preliminary experiments showed that, compared with the normal group, there was no significant change in the protein level of PSD95 in any sham group (6 h and 7 days), suggesting that sham treatment did not affect the protein level of PSD95. The rats in the sham group were sacrificed at 12 h after physiological saline injection. The ICH group was sacrificed at the indicated time points (6 h, 12 h, 24 h, 48 h, 72 h and 7 days). Brain tissues were sampled 1 mm away from the hematoma for western blot to avoid potential red blood cell contamination (Figure 1(b)).

In experiment 2, 144 rats (159 rats were used, 144 survived) were randomly divided into four groups:

sham, ICH, ICH + Vehicle and ICH + Tat-NR2B9c ( $n = 36$  for each group). The second part of the experiment aims to study the role of PSD95 in ICH-induced SBI and the possible mechanism. At 0.5 h after ICH onset, the rats in the ICH + Tat-NR2B9c group received Tat-NR2B9c 2.6 mg/kg (MedChem Express, HY-P0117) by tail vein injection.<sup>27,28</sup> The rats in the ICH + vehicle group were injected with the same volume of saline. At 24 h after ICH, six rats per group were exsanguinated and used to isolate brain tissues for protein extraction (western blot analysis and immunoprecipitation analysis), RNA extraction (RT-PCR analysis) and paraffin section preparation (terminal deoxynucleotidyl transferase-mediated dUTP nick end labeling (TUNEL) staining and fluoro-jade B (FJB) staining). Another six rats per group were used for quick frozen-section preparation for *in situ* zymography. At 72 h after ICH onset, six rats were used for neurological deficit score and brain edema evaluation, and all the serum was collected for enzyme-linked immunosorbent assay (ELISA) to evaluate inflammatory response. The remaining 18 rats per group were subjected to the Morris water maze test during days 22–26 after ICH onset (Figure 1(c)). The rats subjected to the Morris water maze test received Tat-NR2B9c 2.6 mg/kg by tail vein injection once every 3 days. For Morris water maze test, Tat-NR2B9c started to be given at 0.5 h after ICH onset once every 3 days until the rats were sacrificed.

In *in vitro* experiments, neurons were exposed to 20  $\mu$ M OxyHb to mimic the ICH condition. Tat-NR2B9c was used at 0.5  $\mu$ M *in vitro*.

### Antibodies

For details, please see the supplementary material.

### Double immunofluorescent labeling

First, double labeling was performed for PSD95/NeuN to detect the protein level of PSD95 in neurons in the cortex around the hematoma. The fluorescence intensity of PSD95 in NeuN-positive cells was calculated. Second, double labeling was also performed to test the interaction between PSD95 and its binding partners. The patch of protein colocalization means the protein interaction. To exclude the effects of exposure time and background on the result, unified exposure time was performed in an independent test, and the fluorescence intensity of the control group was normalized to 1.0. Normal IgG served as negative control for background removal (data not shown). Sections were observed using a fluorescence microscope (Olympus BX50/BX-FLA/DP70; Olympus Co., Tokyo, Japan). The fluorescence intensity was

analyzed using the ImageJ program (NIH, Bethesda, MD, USA).

### Western blot assay

Western blot assay was performed as described previously.<sup>29</sup> Briefly, the brain samples were cut and dissected using a brain chisel, and mechanically lysed in the lysis buffer for western blot containing phenylmethylsulfonyl fluoride (Beyotime Institute of Biotechnology, Shanghai, China). The protein concentrations were measured by the bicinchoninic acid (BCA) method using an enhanced BCA protein assay kit (Beyotime Institute of Biotechnology). Protein samples (20  $\mu$ g/lane) were loaded on a 12% SDS-polyacrylamide-gel, separated, and electrophoretically transferred to a polyvinylidene difluoride membrane (Millipore, Billerica, MA), which was blocked with 5% bovine serum albumin (Biosharp, Hefei, China) for 1 h at room temperature. The membrane was then incubated overnight at 4°C with primary antibodies and subsequently with the corresponding secondary antibody. Finally, the signals were detected using an ECL kit. ImageJ software was used to analyze optical density of bands.

### RT-PCR

RT-PCR was performed as described previously.<sup>30</sup> Briefly, total RNA was extracted with RNA Trizol (15596-026; Invitrogen Life Technologies, Carlsbad, CA, USA). Next, RNA was reverse transcribed to complementary DNA (cDNA) using the RevertAid First Strand cDNA Synthesis Kit (K1622; Fermentas/Thermo Fisher Scientific, Inc., Rockford, IL, USA). RT-PCR was performed using DreamTaq Green PCR Master Mix (K1081; Thermo Fisher Scientific, Inc., San Jose, CA, USA). GAPDH served as loading controls. All PCR reactions were performed with a GeneAmp PCR system 2004 (Perkin Elmer, Waltham, MA, USA). The PCR products were separated on 1% agarose gel, and the relative densitometry intensity of the bands was quantitated using ImageJ software and normalized to the loading control.

### FJB staining

FJB staining was performed as described previously.<sup>31,32</sup> For details, please see the supplementary material.

### TUNEL + NeuN double standard fluorescent staining

TUNEL staining was performed as described previously.<sup>21</sup> For details, please see the supplementary material.

## ELISA

The concentrations of interleukin (IL)-1 $\beta$  and IL-17 in serum were determined by corresponding ELISA kits (Cat. RA20422 for IL-1 $\beta$  and Cat. RA20117 for IL-17, Bio-Swamp). These assays were performed according to the manufacturer's instructions, and the data were expressed relative to standard curves prepared for them.

## Immunoprecipitation analysis

Immunoprecipitation tests were performed as reported previously.<sup>21</sup> For details, please see the supplementary material.

## Neurological impairment

At 72 h after ICH, the six rats in the experiment 2 were examined for behavioral impairment using a previously published scoring system and monitored for appetite, activity, and neurological defects.<sup>33</sup>

## Morris water maze

The Morris water maze test was performed as described previously.<sup>34,35</sup> Briefly, rats were trained in the Morris water maze on days 3 to 6 post-ICH (four trials per day). Swimming speed, latency and swim path length were recorded. For details, please see the supplementary material.

## In situ zymography

MMP-2/9 activity was tested on frozen section by in situ zymography kit (GMS80062.2, GENMED). This assay was performed according to the manufacturer's instructions, and the fluorescence intensity was quantified by ImageJ software. The fluorescence intensity of the sham group was normalized to 1.0.

## Gelatin gel zymography

Gel zymography was performed as described previously.<sup>36</sup> A mixture of human MMP-2 and MMP-9 (Chemicon, Hofheim, Germany) was used as positive control.

## Statistical analysis

GraphPad Prism 5 was used for all statistical analysis. Neurobehavioral scores were shown as median with interquartile range. All the other data are presented as mean  $\pm$  SD. Frequency distribution for the neurobehavioral score assay. One-way ANOVA for

multiple comparisons and Student–Newman–Keuls post hoc test were used to determine the differences among all groups;  $p < 0.05$  was considered to be significant.

## Results

### General observations

The body temperature, mean arterial pressure, and body weight of rats in each experimental group did not change significantly (Supplementary Figure 1). The mortality rate of rats in the normal and sham group was 0% (0/42 rats), and in the ICH group, it was 11.8% (17/144 rats).

### ICH induced a decrease in the protein level of PSD95 in rat brain

Compared with the sham group, the results of immunofluorescence double staining showed that the protein level of PSD95 in neurons in the cortex around hematoma was significantly decreased at 6 h, reached the lowest point at 12 h, gradually picked up after 24 h, and then fell again at 72 h after ICH (Figure 2(a) and (b)). Western blot assay further showed the same trend in the protein level of PSD95 in the cortex around hematoma (Figure 2(c)). Next, a time course study for the expression of PSD95 after ICH was performed by RT-PCR (Figure 2(d)). The mRNA level of PSD95 in the cortex around hematoma was significantly decreased from 6 h after ICH onset and then recovered to the levels in the sham group after 48 h. Based on these results, we found that the decrease in the protein level of PSD95 at 12 h was due to the ICH-induced decrease in the transcription of PSD95.

### ICH increased the interaction between PSD95 and NR2B-nNOS and inhibited the interaction between PSD95 and neurexin-1–neuroligin-1

We examined the interaction of PSD95 with NR2B-nNOS or neurexin-1–neuroligin-1 by co-immunoprecipitation and double immunofluorescence staining at 24 h after ICH. The results of co-immunoprecipitation showed that the formation of PSD95-NR2B-nNOS complex was significantly increased in the brain tissue of the ICH group compared with the sham group, while the formation of PSD95-neurexin-1–neuroligin-1 complex was significantly reduced (Figure 3(a) and (b)). There were similar trends of the co-localizations of PSD95/NR2B/nNOS and PSD95/neurexin-1/neuroligin-1 in cultured neurons treated with OxyHb (Figure 3(c)).

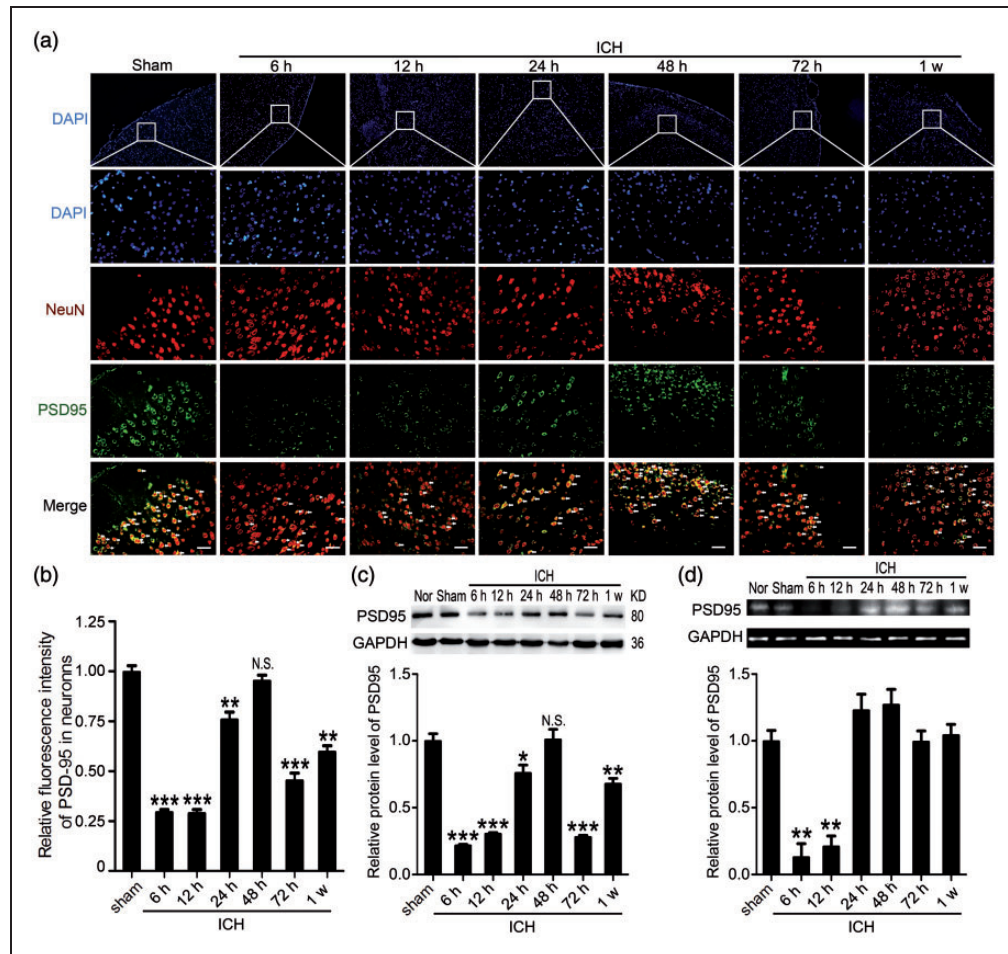


**Figure 2.** The protein levels of PSD95 in neuronal cells after ICH. (a) Double immunofluorescence analysis was performed with antibody for PSD95 (green) and neuronal cell marker (red) in peri-hematoma cortex. Nuclei were fluorescently labeled with 4'-6-diamidino-2-phenylindole (DAPI) (blue). Representative images of the sham and ICH time course groups are shown. Scale bar = 20 μm. (b) The relative fluorescent intensity of PSD95 in neuronal cells is shown below. (c) Western blot analysis and quantification of the protein level of PSD95 in brain tissue. The relative levels were expressed relative to glyceraldehyde-3-phosphate dehydrogenase (GAPDH) protein levels and normalized to the sham group. (d) Reverse transcription polymerase chain reaction (RT-PCR) assay of the messenger RNA (mRNA) levels of PSD95 in brain tissue around hematoma at indicated times after ICH. Relative mRNA levels of PSD95 were calculated based on densitometry analysis. The mean values of the mRNA levels of PSD95 in sham group were normalized to 1.0. In (b), (c), and (d), all values are mean ± SD, \* $p < 0.05$ , \*\* $p < 0.01$ , \*\*\* $p < 0.001$  compared with sham group. N.S. indicates no significant difference,  $n = 6$ .

PSD95: postsynaptic density protein-95; ICH: intracerebral hemorrhage; SD: standard deviation.

### Tat-NR2B9c inhibited the formation of PSD95-NR2B-nNOS complex induced by ICH

By co-immunoprecipitation and double immunofluorescence staining, we then examined the effects of Tat-NR2B9c intervention on the interaction of PSD95 with NR2B-nNOS or neuroligin-1–neuroligin-1 at 24 h after ICH. The results of co-immunoprecipitation showed that the PSD95-NR2B-nNOS complex was significantly decreased in the Tat-NR2B9c-treated group compared with the vehicle group, while the PSD95-neuroligin-1–neuroligin-1 complex was significantly increased by Tat-NR2B9c intervention (Figure 4(a) and (b)).

Furthermore, in vitro double immunofluorescence staining also showed a consistent trend (Figure 4(c)).

### In vivo rescue effects of Tat-NR2B9c intervention on ICH-induced SBI

To examine the effects of Tat-NR2B9c intervention on SBI induced by ICH, we used TUNEL and FJB staining to detect the effect of Tat-NR2B9c on neuronal death and degeneration in the brain at 24 h after ICH. Compared with the sham group, the number of TUNEL- and FJB-positive cells increased significantly in the ICH group, while the number of TUNEL- and

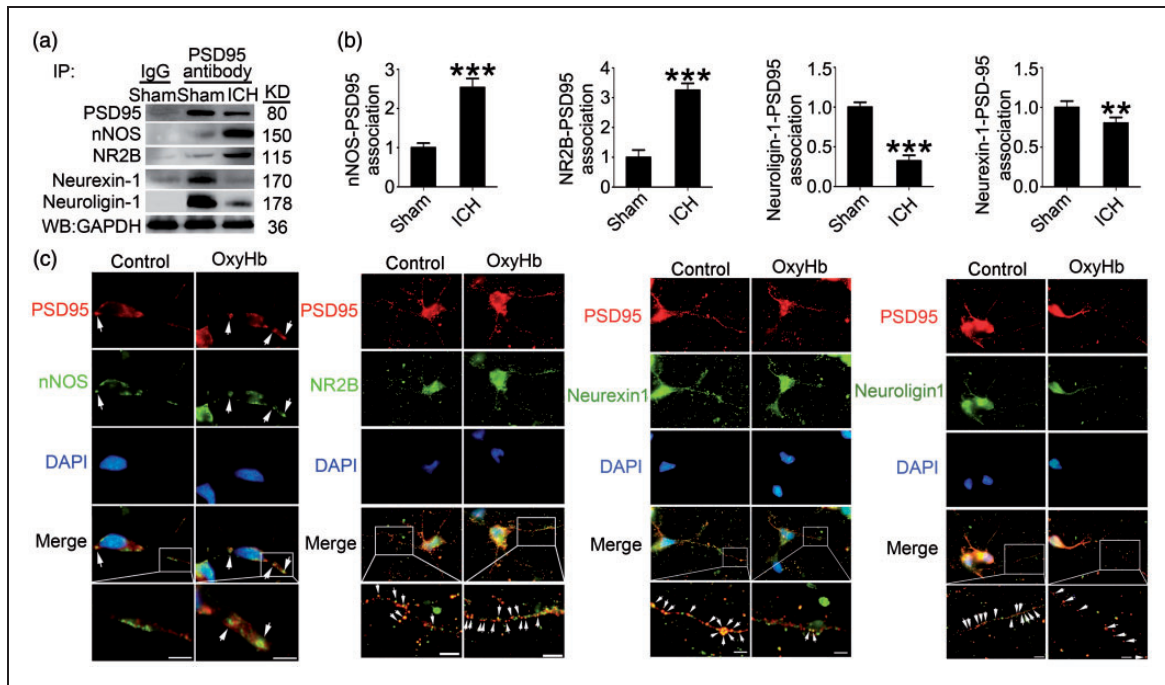


**Figure 3.** PSD95 and NR2B-nNOS, PSD95 and neurexin–neuroigin interacts after ICH. (a) IP of brain tissue whole protein with indicated treatments. Western blots of IP with PSD95 antibody showed the interactions between nNOS, NR2B, neurexin-1 or neuroigin-1, and PSD95. (b) The relative levels of nNOS/NR2B/neurexin-1/neuroigin-1 immunoprecipitated by PSD95. The relative levels were normalized to the sham group. The y-axis is the fold of sham group. Data are expressed as mean  $\pm$  SD. \*\*\* $p < 0.01$ , \*\*\* $p < 0.001$  compared with sham group,  $n = 6$ . (c) Double immunofluorescence analysis was performed with antibody for nNOS (green), GluN2B (green), neurexin-1 $\beta$  (green), neuroigin-1 (green), and PSD95 (red) in cultured neurons exposed to indicated treatments. Nuclei were fluorescently labeled with DAPI (blue). Representative images of the control and oxyHb (24 h) groups are shown. Scale bar = 10  $\mu$ m. PSD95: postsynaptic density protein-95; ICH: intracerebral hemorrhage; nNOS: neurotransmitter nitric oxide synthase; IP: immunoprecipitation; SD: standard deviation.

FJB-positive cells was significantly decreased by Tat-NR2B9c intervention (Figure 5(a) to (e)). Then, the activation of caspase-3 in the brain tissue around the hematoma was detected by western blotting. The results showed that the Tat-NR2B9c intervention inhibited ICH-induced brain cell apoptosis (Figure 5(f) and (g)). Next, compared with the sham group, there was a significant increase in the brain content of albumin in the ICH group, and this was significantly decreased by Tat-NR2B9c treatment (Figure 5(f) and (h)). In addition, brain water content was found to be significantly higher in brain samples of the ICH (72 h) group than in the sham group. Brain water content was lower in rats treated with Tat-NR2B9c than in the vehicle group (Figure 5(i)). And, during harvesting the brain tissue, we quantified the hematoma volume of each group exposed to ICH insults and found that no significant changes in hematoma volume were detected among ICH group, ICH + vehicle group, and ICH + Tat-NR2B9c group (data not shown), suggesting that Tat-NR2B9c did not affect hematoma volume. Finally, inflammatory cytokines, including IL-1 $\beta$  and

IL-17, were found to be significantly higher in the serum of the ICH group than in that of the sham group. Compared with the ICH + vehicle group, the mean inflammatory cytokine contents were significantly lower in the ICH + Tat-NR2B9c group (Figure 5(j)).

### Tat-NR2B9c rescued cognitive impairment caused by ICH

To examine whether Tat-NR2B9c benefits ICH outcome, the Morris water maze was used to evaluate the neurobehavioral disorder in rats during days 22–26 after ICH onset (Figure 6(a)). Compared with the sham group, the escape latency and swimming distance of the ICH group were significantly increased. Compared with the vehicle group, the escape latency (Figure 6(b)) and swimming distance (Figure 6(c)) were significantly reduced in the Tat-NR2B9c intervention group, suggesting that Tat-NR2B9c exerted significant rescue effects on cognitive impairment following ICH. In addition, we tested Tat-NR2B9c on behavioral outcome in the collagenase ICH model at 72 h

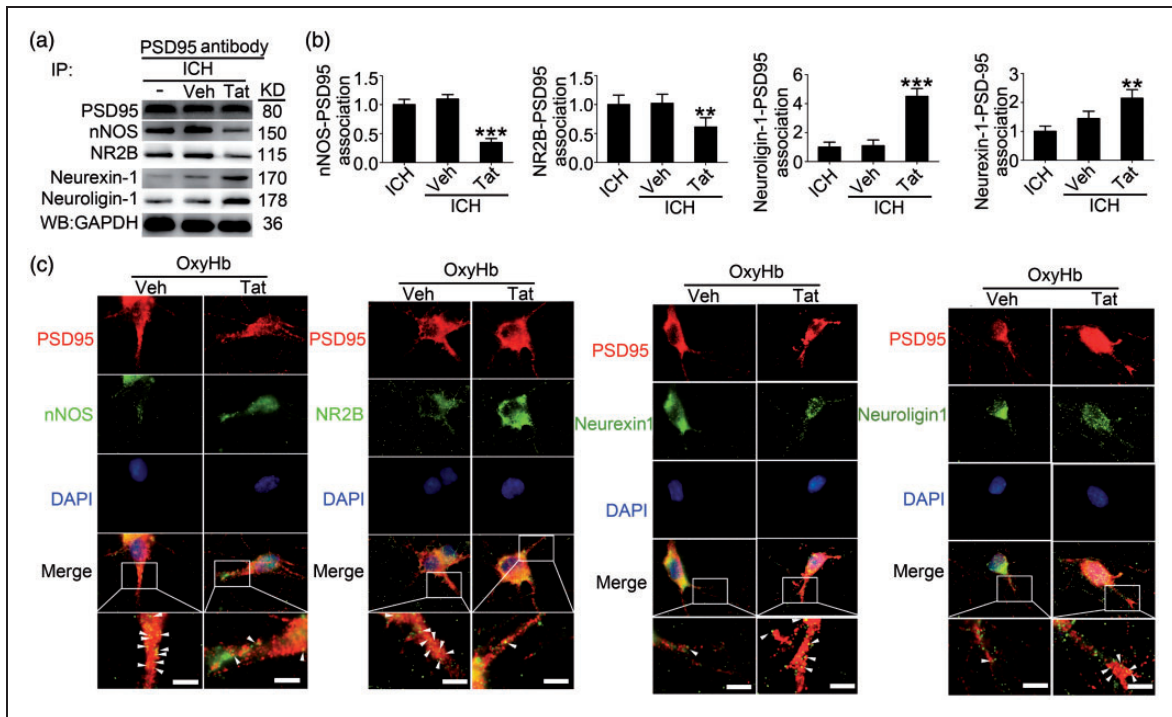


**Figure 4.** Tat-NR2B9c affects PSD95-NR2B-nNOS complex and PSD95-neurexin-neurologin complex formation after ICH. (a) IP of brain tissue whole protein with indicated treatments. Western blots of IP with PSD95 antibody showed the interactions between nNOS, NR2B, neurexin-1 or neurologin-1, and PSD95. (b) The relative levels of nNOS/NR2B/neurexin-1/neurologin-1 immunoprecipitated by PSD95. The relative levels were normalized to the sham group. The y-axis is the fold of sham group. Data are expressed as mean  $\pm$  SD. \*\* $p < 0.01$ , \*\*\* $p < 0.001$  compared with ICH + Vehicle group,  $n = 6$ . (c) Double immunofluorescence analysis was performed with antibody for nNOS (green), GluN2B (green), neurexin-1 (green), neurologin-1 (green), and PSD95 (red) in cultured neurons exposed to indicated treatments. Nuclei were fluorescently labeled with DAPI (blue). Representative images of the oxyHb + Vehicle and oxyHb + Tat-NR2B9c groups are shown. Scale bar = 10  $\mu$ m. PSD95: postsynaptic density protein-95; ICH: intracerebral hemorrhage; nNOS: neurotransmitter nitric oxide synthase; IP: immunoprecipitation; SD: standard deviation.

after ICH onset (Figure 6(d)). Compared with sham group, ICH rats showed a significant damage in neurobehavioral ability, while Tat-NR2B9c exerted a rescue effect on the neurobehavioral function. Autologous blood ICH model showed a same trend (Figure 6(e)).

#### Tat-NR2B9c inhibited the activation of MMP2/9 induced by ICH

We used in situ gelatin zymography to detect the effect of Tat-NR2B9c on the activity of MMP2/9 after ICH. Compared with the sham group, the activity of MMP2/9 in the brain tissue of the ICH group increased significantly after 24 h, and this was significantly inhibited by Tat-NR2B9c treatment. Thus, Tat-NR2B9c effectively reduced the activation of MMP2/9 induced by ICH accompanied by inhibiting the formation of PSD95-NR2B-nNOS complex (Figure 7(a) and (b)). As in situ zymography cannot distinguish between MMP-2 and -9, we performed gelatin gel zymography to

assess the activation status of MMP-2 and -9 specifically. As shown in Figure 7(c) and (d), both pro-MMP-9 and pro-MMP-2 were present in all group. After ICH insults, a second band corresponding to the activated form of MMP-9 appeared. Unlike MMP-9, no activated MMP-2 were detected in ICH brains, suggesting that during ICH MMP-9, but not MMP-2 is activated. Furthermore, with Tat-NR2B9c treatment, MMP-9 activity during ICH was significantly blocked compared with ICH + vehicle group.

#### Discussion

Recent studies have found that SBI is often accompanied by neuronal damage and apoptosis after ICH.<sup>10</sup> Cerebral structure and functional reorganization after ICH is beneficial to the recovery of neurological function, and the fundamental mechanism of brain structure function reorganization is brain plasticity.<sup>9</sup> The plasticity of the brain tissue is due in part to the increase in the number of synapses and the

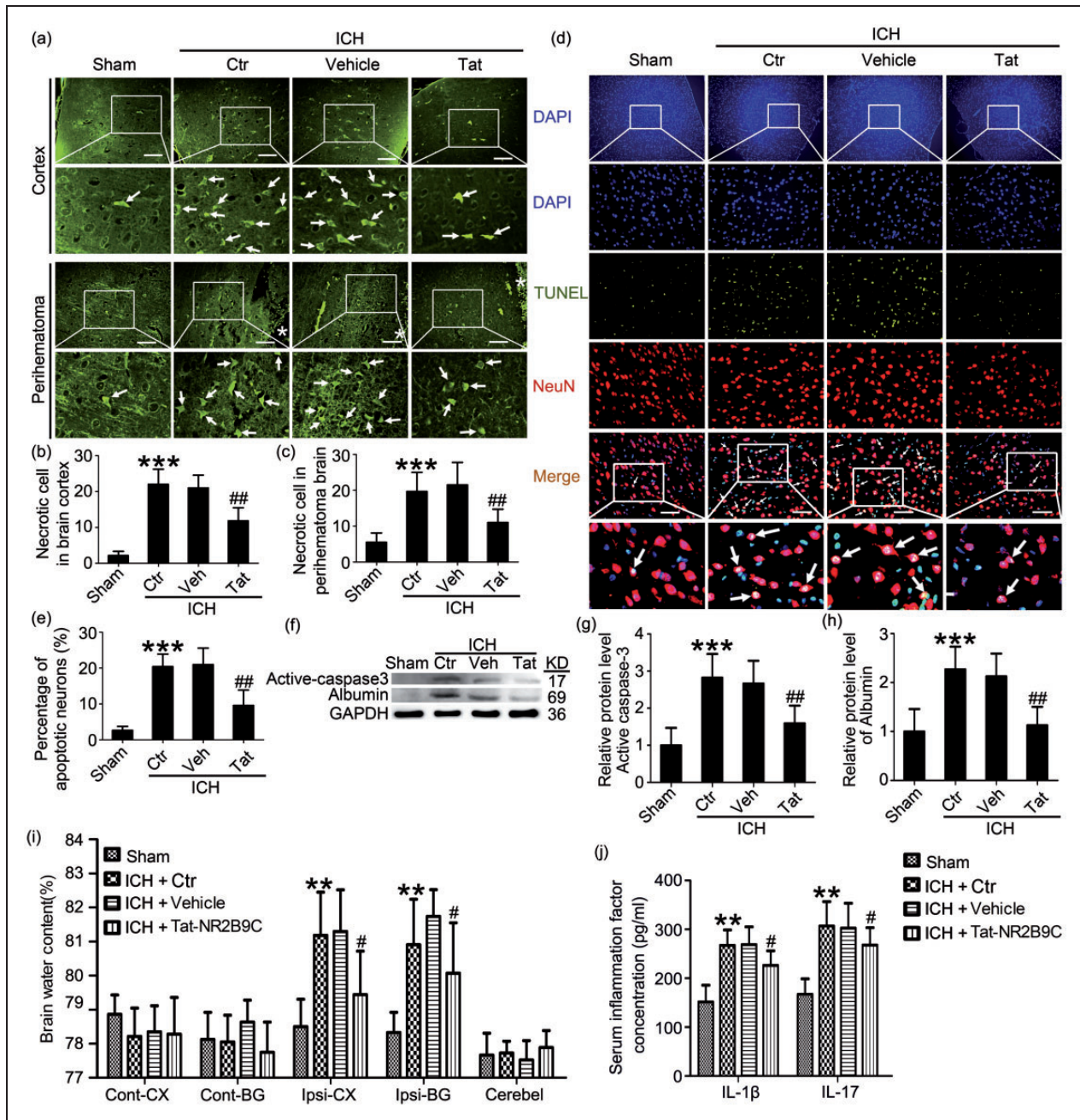


**Figure 5.** Tat-NR2B9c plays a rescue role in ICH-induced SBI. (a) FJB staining (green) shows neuronal degradation both in brain cortex and peri-hematoma brain. Scale bar = 100 mm. Arrows point to FJB-positive cells. FJB-positive cells/mm<sup>2</sup> were quantified in brain cortex (b) and peri-hematoma brain (c). (d) Double staining for neuronal cell marker (red) and TUNEL (green) counterstained with DAPI (blue) was performed. Representative images of sham group, ICH + control (24 h) group, ICH + vehicle (24 h) group, and ICH + Tat-NR2B9c (24 h) group are shown. Arrows point to apoptotic neurons, namely NeuN/TUNEL-positive cells. Scale bar = 20 mm. Percentage of TUNEL-positive neurons is shown (e). Western blot analysis and quantification of the protein level of active-caspase3 and albumin in brain tissue ((f)–(h)). Quantitative levels of protein levels of active caspase 3 and albumin are shown (g) and (h). (i) Bar graphs showing the effects of Tat-NR2B9c on brain water content. (j) ELISA assay of the contents of IL-1 $\beta$  and IL-17 in serum. In (b), (c), (e), (g), (h), (i), and (j), data are expressed as mean  $\pm$  SD. \*\*\* $p$  < 0.01, \*\*\*\* $p$  < 0.001 vs. sham group, # $p$  < 0.05, ### $p$  < 0.01 vs. ICH + Vehicle group,  $n$  = 6. In (g) and (h), the relative levels were expressed relative to GAPDH protein levels and normalized to the sham group.

ICH: intracerebral hemorrhage; SBI: secondary brain injury; FJB: fluoro-Jade B; TUNEL: terminal deoxynucleotidyl transferase-mediated dUTP nick end labeling; ELISA: enzyme-linked immunosorbent assay; IL: interleukin; Cont: contralateral; Ipsi: ipsilateral; CX: cortex; BG: basal ganglia; Cerebel: cerebellum.

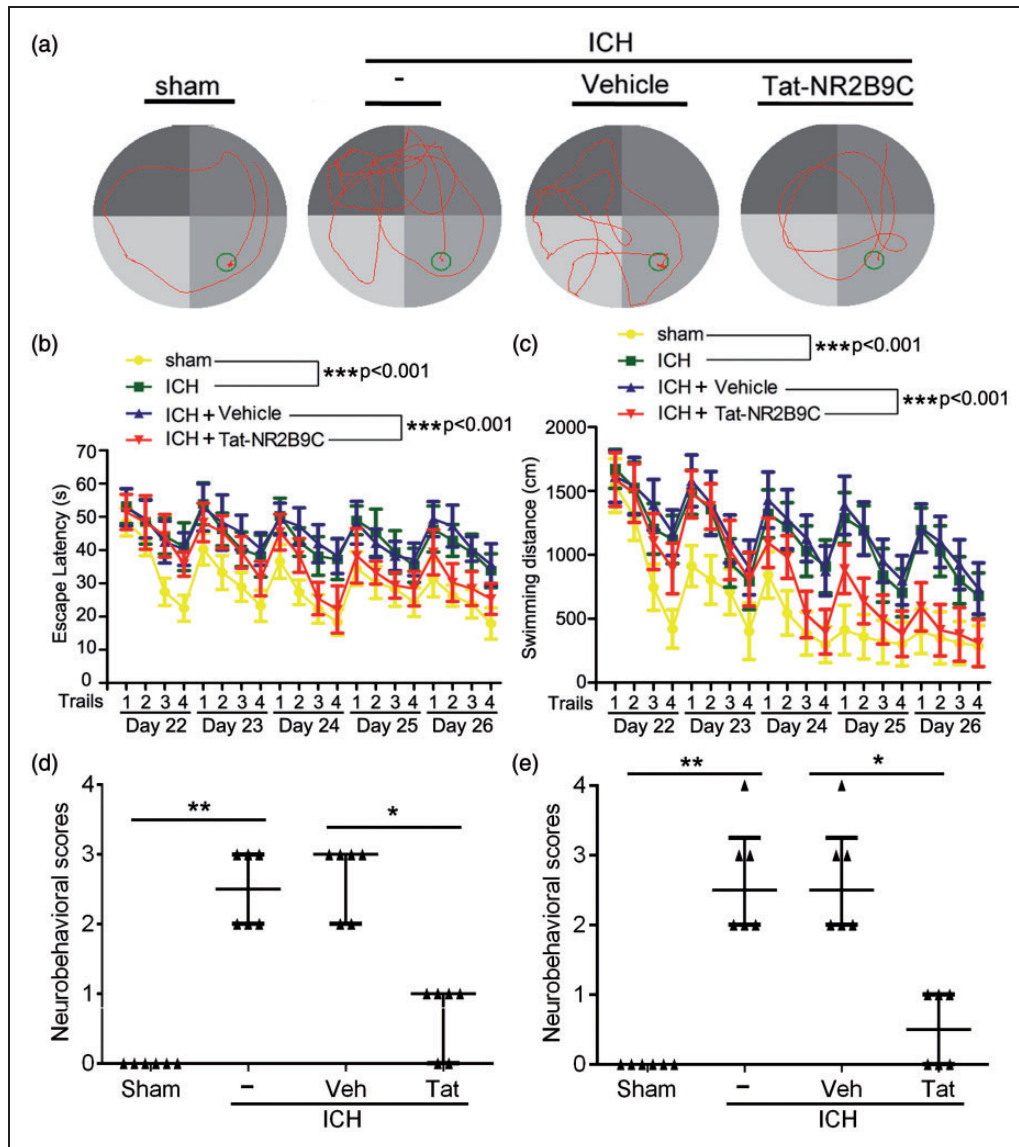


**Figure 6.** Morris water maze test and neurobehavioral scores. (a) Morris water maze test in rats during days 22–26 after ICH onset. Comparison of typical trajectories for each group of space exploration was shown. (b) Escape latency and (c) swim path length of 4 trials per day for 5 days,  $n = 18$ . Neurobehavioral scores were tested at 72 h after surgery in collagenase ICH model (d) or in autologous blood ICH model (e). In (d) and (e), \* $p < 0.05$ , \*\* $p < 0.01$ ,  $n = 6$ . ICH: intracerebral hemorrhage.

enhancement of synaptic function. The increase in the number of synapses and the enhancement of function can increase the association between neurons, inhibit the initiation of apoptosis, and enhance the activity of peripheral neurons in cerebral hemorrhage.<sup>13</sup> Some studies have attempted to achieve the treatment of nervous system-related diseases by altering postsynaptic membrane-associated proteins.<sup>13,21,37</sup> Previously, our study found that some proteins in the postsynaptic membrane density region were affected by hemorrhagic brain disease.<sup>21</sup> In previous studies, over-expression of the

synaptic-associated proteins neurexin-1 and neuroligin-1 could increase the interaction between them and the formation of excitatory synapses, and could improve hemorrhagic brain disease-induced cognitive dysfunction, whereas knockdown of neurexin-1 and neuroligin-1 led to the opposite effect.<sup>21</sup> In this study, we further explore the role of the neurexin-1 and neuroligin-1-related protein PSD95 and its intervention in cognitive function after ICH.

In this study, we first found that the expression of PSD95 was decreased after ICH. However,

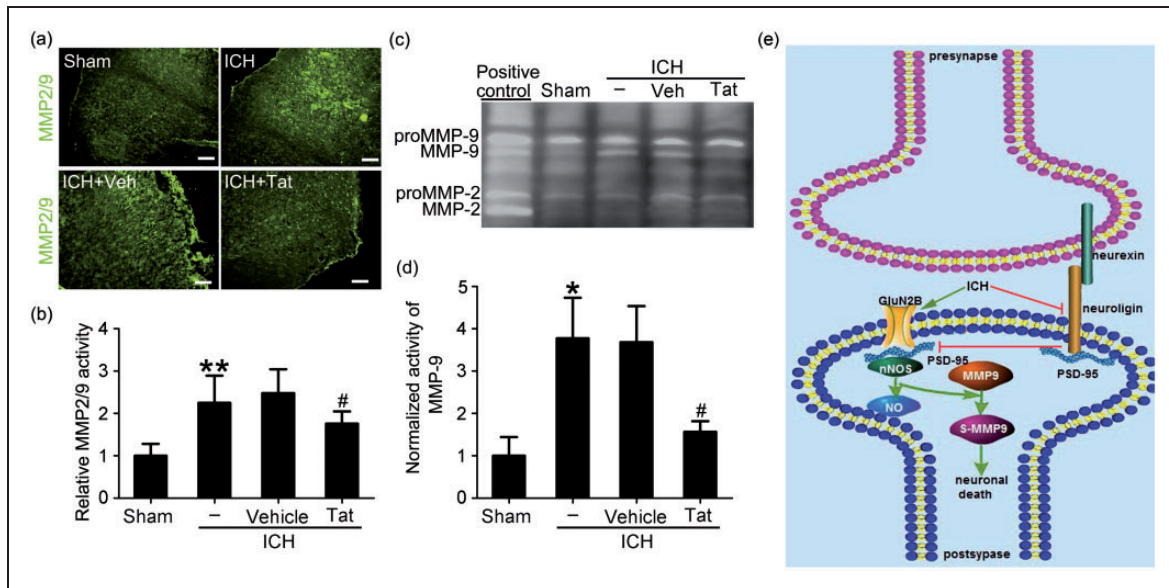


**Figure 7.** The effect of Tat-NR2B9c on the activity of MMP2/9 in brain tissue and the roles of PSD95 in SBI after ICH. (a) In situ gelatin zymography assay of MMP2/9 activity (green), as well as quantitative analysis (b). In (b), data are expressed as mean  $\pm$  SD.  $**p < 0.01$  vs. sham group,  $\#p < 0.05$  vs. ICH + Vehicle group. (c) Gelatin gel zymography assay of MMP-2/9 activity (d) Densitometric quantification showing the normalized activity of MMP-9. Data = mean  $\pm$  SD,  $n = 6$ .  $*p < 0.05$  vs. sham group,  $\#p < 0.05$  vs. ICH + Vehicle group. (e) The mechanism of PSD95 in SBI after ICH. After ICH, the excitatory glutamate is released in large quantities, the NMDA receptor is activated, the PSD95-NR2B-nNOS complex is increased, nNOS and MMP9 are activated, and the neuroligin-neurexin-PSD95 formation is inhibited, affecting the formation of synapses, differentiation, maturation, and remodeling, leading to behavioral disorders in rats.

PSD95: postsynaptic density protein-95; ICH: intracerebral hemorrhage; nNOS: neurotransmitter nitric oxide synthase; SD: standard deviation; MMP: matrix metalloproteinase; SBI: secondary brain injury.

PSD95-NR2B-nNOS complex increased and neuroligin-1-neurologlin-1-PSD95 complex decreased in rats' brain tissue after ICH. The formation of PSD95-NR2B-nNOS complex may promote the production of nitric oxide, which promotes excessive S-nitrosylation and activation of MMP9, and induces neuronal death as described previously.<sup>20</sup> Tat-NR2B9c can reduce the production of PSD95-NR2B-nNOS complex by reducing the interaction between PSD95 and NR2B-nNOS, which alleviates neuronal death induced by ICH. On the other hand, Tat-NR2B9c contributes to the improvement of behavior caused by ICH by promoting the formation of neuroligin-1-neurologlin-1-PSD95 complex (Figure 7(e)).

To prove the cytotoxicity of the Tat-NR2B9c, sham-operated rats were treated with Tat-NR2B9c 2.6 mg/kg by tail vein injection in our preliminary experiments, which is the same dosage of that used in ICH group in this study. We assessed the brains of native and Tat-NR2B9c-injected sham rats by western blot assay of active-caspase 3. The results showed that Tat-NR2B9c treatment at the dosage used in this study did not induce significant change in brain cell apoptosis (data not shown), suggesting that there was no obvious side effects of Tat-NR2B9c at the dosage used in this study.

The BBB acts as a selective permeability barrier between circulating blood and the central nervous system. BBB disruption occurs and contributes to the progression of ICH-induced SBI.<sup>38</sup> However, there is evidence that BBB disruption could promote the access of some drugs to the immediate environment around the disruption.<sup>39</sup> In this sense, BBB disruption induced by ICH may facilitate Tat-NR2B9c transport across the BBB into the brain. In addition, the PSD95 inhibitor Tat-NR2B9c is a short peptide chain containing 20 amino acids formed by the fusion of 11-amino-acid peptide chains of HIV-1 Tat with the 9-amino-acid peptide chains of the NMDA receptor subunit NR2B carboxy terminus. The peptide chains of HIV-1 Tat contain Arg-Lys-Lys-Arg-Arg-Gln-Arg-Arg-Arg, which exerts as a transmembrane domain and enables the fusion protein to cross the blood-brain barrier and reach the brain.<sup>40</sup> Furthermore, Tat-NR2B9c conjugated with fluorophore dansyl chloride showed that Tat-NR2B9c application via intraperitoneal injection could be delivered into the brain in intact C57BL/6 mice and transduce into neurons via intracellular peptide uptake,<sup>27</sup> and intravenous infusion of Tat-NR2B9c (2.6 mg/kg) could exert neuroprotection and improve functional outcome after ischemic stroke.<sup>28</sup>

It was reported that, when cultured neurons were exposed to Tat-NR2B9c, Tat-NR2B9c accumulation was detectable in neurons within 10 min, peaked during the next 20 min, and remained detectable for 5 h after washing the peptide from the bath.<sup>27</sup> In addition, neuroprotection of Tat-NR2B9c via regulating PSD95 binding properties was detectable in cultured neurons exposed to an NMDA challenge within 24 h of Tat-NR2B9c application.<sup>27</sup> Furthermore, a one-time intraperitoneal injection of Tat-NR2B9c at 1 h after middle cerebral artery occlusion onset significantly reduced the volume of total cerebral infarction and improved the neurological scores at 24 h after surgery.<sup>27</sup> Here, we chose a one-time intravenous infusion of Tat-NR2B9c for evaluating MMP-2/9 activity at 24 h after ICH onset. In this study, we focused only on the effects of Tat-NR2B9c on PSD95 binding properties in neurons and ignored different MMP-2/9 activity-positive cell types. However, astrocytes and neutrophils contribute to the MMP-2/9 activity in stroke models,<sup>41</sup> and we will further study the effect of Tat-NR2B9c on astrocytes and neutrophils exposed to ICH insults.

After ICH, glutamate release is increased and intake is reduced, and postsynaptic neuron glutamate receptors are over-activated. Under the stimulation of glutamate, NMDA receptors activate a series of signaling molecules through PSD95 to achieve their toxicity effect. This PSD95 not only anchors the NMDA receptor but also migrates the downstream signaling molecules to the NMDA receptor calcium channel. This promotes  $\text{Ca}^{2+}$  influx and intracellular  $\text{Ca}^{2+}$  overload; activates its target enzyme; produces a large amount of reactive oxygen species, nitric oxide and high activity of nitro compounds, and other harmful substances. This results in the release of inflammatory cytokines, membrane lipid peroxidation, the activation of caspase-3, and finally, neuronal damage and apoptosis.<sup>42,43</sup> Tat-NR2B9c can destroy the interaction between PSD95 and NR2B, and can thereby reduce the subsequent over-nitration of MMPs and reduce the excitotoxicity of neuron.<sup>27</sup> At present, many animal experiments and clinical studies of ischemic stroke have found that Tat-NR2B9c exerts significant neuroprotective effects.<sup>27,28,44</sup> However, whether the inhibition of PSD95 activity by Tat-NR2B9c in ICH also has protective effects, and what the possible mechanisms might be, have rarely been reported.

SBI led to modification of the synaptic response after ICH.<sup>45,46</sup> The synapse, a special cell connection between neurons, is a key part of the exchange of information between neurons.<sup>47</sup> The increase in the number of synapses and the enhancement of synapse function can increase the association between neurons, inhibit the initiation of apoptosis, and enhance the

activity of peripheral neurons in cerebral hemorrhage.<sup>14</sup> Previous studies have shown that the formation of cognition and the signal transduction depend on the interaction of synaptic molecules. In Figure 6, our study confirmed that Tat-NR2B9c improved ICH-induced cognitive impairment. As shown in Figure 4, PSD95 inhibitor Tat-NR2B9c effectively inhibited the interaction between PSD95 and NR2B-nNOS, and promoted the formation of neurexin-1–neuroigin-1-PSD95 complex. Our previous work had clarified the role of neurexin-1 and neuroigin-1 in cognitive disorders after subarachnoid hemorrhage.<sup>21</sup> This study further elucidated the mechanisms underlying the functions of neurexin-1 and neuroigin-1 in hemorrhagic stroke.

The current study has some limitations. We tested only the effects of OxyHb on the distribution of PSD95, but the potential effects of other hematoma components also should be considered. In addition, primary neuronal culture lacks cell–cell interaction and therefore could not mimic *in vivo* conditions completely. Next, only focusing on the effect of Tat-NR2B9c in the collagenase ICH model is a limitation. The effects of Tat-NR2B9c on brain injury in the blood ICH model will be confirmed in our further study. TUNEL is not specific for apoptosis. In order to elucidate the effect of Tat-NR2B9c on brain cell apoptosis, we also have given a more objective index for apoptosis: western blot assay of active-caspase 3 in this study (Figure 5(f) and (g)). However, ferroptosis has been shown to occur in ICH models.<sup>48,49</sup> Whether Tat-NR2B9c can inhibit ferroptotic cell death in this ICH model need further study. Finally, based on STAIR criteria, these results should be replicated in a second species, and sex differences should be considered. We will explore these other considerations in further studies.

## Conclusion

This study demonstrated for the first time that PSD95 inhibitor Tat-NR2B9c can reduce the production of PSD95-NR2B-nNOS and reduce the death of neurons. At the same time, the production of neurexin-1–neuroigin-1-PSD95 complex is increased and the behavioral cognitive disorder is improved. Thus, PSD95 plays a key role in SBI after ICH. The inhibitor of PSD95 might be a promising treatment target for cognitive dysfunction after ICH.

## Funding

The author(s) disclosed receipt of the following financial support for the research, authorship, and/or publication of this article: Project of Jiangsu Provincial Medical Innovation

Team (CXTDA2017003), Jiangsu Provincial Medical Youth Talent (QNRC2016728), Suzhou Key Medical Center (Szzx201501), National Natural Science Foundation of China (81471196), Natural Science Foundation of Jiangsu Province (BK20170363), Scientific Department of Jiangsu Province (BE2017656), and Suzhou Government (LCZX201601).

### Declaration of conflicting interests

The author(s) declared no potential conflicts of interest with respect to the research, authorship, and/or publication of this article.

### Authors' contributions

GC and ZW conceived and designed the study. ZW and ZC performed the experiments and wrote the paper. Junjie Y and ZY assisted in the use of the laser scanning confocal microscope. Jia Y and XD helped conduct the literature review. HS and HL reviewed and edited the manuscript. All authors read and approved the manuscript.

### Supplementary material

Supplementary material for this paper can be found at the journal website: <http://journals.sagepub.com/home/jcb>

### ORCID iD

Gang Chen  <http://orcid.org/0000-0002-0758-1907>

### References

1. Qureshi AI, Mendelow AD and Hanley DF. Intracerebral haemorrhage. *Lancet* 2009; 373: 1632–1644.
2. Lan X, Han X, Li Q, et al. Modulators of microglial activation and polarization after intracerebral haemorrhage. *Nat Rev Neurol* 2017; 13: 420–433.
3. Urday S, Kimberly WT, Beslow LA, et al. Targeting secondary injury in intracerebral haemorrhage–perihematomal oedema. *Nat Rev Neurol* 2015; 11: 111–122.
4. Li Q, Wan J, Lan X, et al. Neuroprotection of brain-permeable iron chelator VK-28 against intracerebral hemorrhage in mice. *J Cereb Blood Flow Metab* 2017; 37: 3110–3123.
5. Xi G, Strahle J, Hua Y, et al. Progress in translational research on intracerebral hemorrhage: is there an end in sight? *Prog Neurobiol* 2014; 115: 45–63.
6. Rostamian S, Mahinrad S, Stijnen T, et al. Cognitive impairment and risk of stroke: a systematic review and meta-analysis of prospective cohort studies. *Stroke* 2014; 45: 1342–1348.
7. Zhao XR, Gonzales N and Aronowski J. Pleiotropic role of PPARgamma in intracerebral hemorrhage: an intricate system involving Nrf2, RXR, and NF-kappaB. *CNS Neurosci Ther* 2015; 21: 357–366.
8. Duan XC, Wang W, Feng DX, et al. Roles of autophagy and endoplasmic reticulum stress in intracerebral hemorrhage-induced secondary brain injury in rats. *CNS Neurosci Ther* 2017; 23: 554–566.
9. Tamakoshi K, Kawanaka K, Onishi H, et al. Motor skills training improves sensorimotor dysfunction and increases microtubule-associated protein 2 mRNA expression in rats with intracerebral hemorrhage. *J Stroke Cerebrovasc Dis* 2016; 25: 2071–2077.
10. Wang Z, Chen Z, Yang J, et al. Identification of two phosphorylation sites essential for annexin A1 in blood-brain barrier protection after experimental intracerebral hemorrhage in rats. *J Cereb Blood Flow Metab* 2017; 37: 2509–2525.
11. Ariesen MJ, Claus SP, Rinkel GJ, et al. Risk factors for intracerebral hemorrhage in the general population: a systematic review. *Stroke* 2003; 34: 2060–2065.
12. Poels MM, Vernooij MW, Ikram MA, et al. Prevalence and risk factors of cerebral microbleeds: an update of the Rotterdam scan study. *Stroke* 2010; 41: S103–S106.
13. Mokrushin AA and Pavlinova LI. Effects of the blood components on the AMPA and NMDA synaptic responses in brain slices in the onset of hemorrhagic stroke. *Gen Physiol Biophys* 2013; 32: 489–504.
14. Nakayama K, Kiyosue K and Taguchi T. Diminished neuronal activity increases neuron-neuron connectivity underlying silent synapse formation and the rapid conversion of silent to functional synapses. *J Neurosci* 2005; 25: 4040–4051.
15. Keith D and El-Husseini A. Excitation control: Balancing PSD-95 function at the synapse. *Front Mol Neurosci* 2008; 1: 4. DOI: 10.3389/neuro.02.004.2008.
16. Kim E and Sheng M. PDZ domain proteins of synapses. *Nat Rev Neurosci* 2004; 5: 771–781.
17. Jiang B, Li L, Chen Q, et al. Role of glibenclamide in brain injury after intracerebral hemorrhage. *Transl Stroke Res* 2017; 8: 183–193.
18. Rodriguez JA, Sobrino T, Lopez-Arias E, et al. CM352 reduces brain damage and improves functional recovery in a rat model of intracerebral hemorrhage. *J Am Heart Assoc* 2017; 6. DOI: 10.3389/neuro.02.004.2008.
19. Muhammad S, Planz O and Schwaninger M. Increased plasma matrix metalloproteinase-9 levels contribute to intracerebral hemorrhage during thrombolysis after concomitant stroke and influenza infection. *Cerebrovasc Dis Extra* 2016; 6: 50–59.
20. Gu Z, Kaul M, Yan B, et al. S-nitrosylation of matrix metalloproteinases: signaling pathway to neuronal cell death. *Science* 2002; 297: 1186–1190.
21. Shen H, Chen Z, Wang Y, et al. Role of neurexin-1beta and neuroligin-1 in cognitive dysfunction after subarachnoid hemorrhage in rats. *Stroke* 2015; 46: 2607–2615.
22. Sudhof TC. Neuroligins and neurexins link synaptic function to cognitive disease. *Nature* 2008; 455: 903–911.
23. Rosenberg GA, Estrada E, Wesley M, et al. Autoradiographic patterns of brain interstitial fluid flow after collagenase-induced haemorrhage in rat. *Acta Neurochir Suppl (Wien)* 1990; 51: 280–282.
24. de Groot J. The rat hypothalamus in stereotaxic coordinates. *J Comp Neurol* 1959; 113: 389–400.
25. Bederson JB, Pitts LH, Tsuji M, et al. Rat middle cerebral artery occlusion: evaluation of the model and development of a neurologic examination. *Stroke* 1986; 17: 472–476.

26. Pacifici M and Peruzzi F. Isolation and culture of rat embryonic neural cells: a quick protocol. *J Vis Exp* 2012; e3965.
27. Aarts M, Liu Y, Liu L, et al. Treatment of ischemic brain damage by perturbing NMDA receptor-PSD-95 protein interactions. *Science* 2002; 298: 846–850.
28. Cook DJ, Teves L and Tymianski M. Treatment of stroke with a PSD-95 inhibitor in the gyrencephalic primate brain. *Nature* 2012; 483: 213–217.
29. Li H, Gao A, Feng D, et al. Evaluation of the protective potential of brain microvascular endothelial cell autophagy on blood-brain barrier integrity during experimental cerebral ischemia-reperfusion injury. *Transl Stroke Res* 2014; 5: 618–626.
30. Li H, Wang Y, Feng D, et al. Alterations in the time course of expression of the Nox family in the brain in a rat experimental cerebral ischemia and reperfusion model: effects of melatonin. *J Pineal Res* 2014; 57: 110–119.
31. Zhu HT, Bian C, Yuan JC, et al. Curcumin attenuates acute inflammatory injury by inhibiting the TLR4/MyD88/NF-kappaB signaling pathway in experimental traumatic brain injury. *J Neuroinflamm* 2014; 11: 59. DOI: 10.1186/1742-2094-11-59.
32. Lin S, Yin Q, Zhong Q, et al. Heme activates TLR4-mediated inflammatory injury via MyD88/TRIF signaling pathway in intracerebral hemorrhage. *J Neuroinflamm* 2012; 9: 46.
33. Dang B, Li H, Xu X, et al. Cyclophilin A/cluster of differentiation 147 interactions participate in early brain injury after subarachnoid hemorrhage in rats. *Crit Care Med* 2015; 43: e369–e381.
34. Jeon H, Ai J, Sabri M, et al. Learning deficits after experimental subarachnoid hemorrhage in rats. *Neuroscience* 2010; 169: 1805–1814.
35. Wurm F, Keiner S, Kunze A, et al. Effects of skilled forelimb training on hippocampal neurogenesis and spatial learning after focal cortical infarcts in the adult rat brain. *Stroke* 2007; 38: 2833–2840.
36. Bauer AT, Burgers HF, Rabie T, et al. Matrix metalloproteinase-9 mediates hypoxia-induced vascular leakage in the brain via tight junction rearrangement. *J Cereb Blood Flow Metab* 2010; 30: 837–848.
37. Tamakoshi K, Ishida A, Takamatsu Y, et al. Motor skills training promotes motor functional recovery and induces synaptogenesis in the motor cortex and striatum after intracerebral hemorrhage in rats. *Behav Brain Res* 2014; 260: 34–43.
38. Kassner A and Merali Z. Assessment of blood-brain barrier disruption in stroke. *Stroke* 2015; 46: 3310–3315.
39. Banks WA. Drug delivery to the brain in Alzheimer's disease: consideration of the blood-brain barrier. *Adv Drug Deliv Rev* 2012; 64: 629–639.
40. Cooper I, Sasson K, Teichberg VI, et al. Peptide derived from HIV-1 TAT protein destabilizes a monolayer of endothelial cells in an in vitro model of the blood-brain barrier and allows permeation of high molecular weight proteins. *J Biol Chem* 2012; 287: 44676–44683.
41. Hernandez-Guillamon M, Martinez-Saez E, Delgado P, et al. MMP-2/MMP-9 plasma level and brain expression in cerebral amyloid angiopathy-associated hemorrhagic stroke. *Brain Pathol* 2012; 22: 133–141.
42. Sattler R, Xiong Z, Lu WY, et al. Specific coupling of NMDA receptor activation to nitric oxide neurotoxicity by PSD-95 protein. *Science* 1999; 284: 1845–1848.
43. Bell JD, Cho JE and Giffard RG. MicroRNA changes in preconditioning-induced neuroprotection. *Transl Stroke Res* 2017; 8: 585–596.
44. Lai TW, Zhang S and Wang YT. Excitotoxicity and stroke: identifying novel targets for neuroprotection. *Prog Neurobiol* 2014; 115: 157–188.
45. Fiehler J. Cerebral microbleeds: old leaks and new haemorrhages. *Int J Stroke* 2006; 1: 122–130.
46. Nishikawa T, Ueba T, Kajiwara M, et al. Cerebral microbleeds in patients with intracerebral hemorrhage are associated with previous cerebrovascular diseases and white matter hyperintensity, but not with regular use of antiplatelet agents. *Neurol Med Chir (Tokyo)* 2009; 49: 333–338; discussion 8–9.
47. Reimann MW, Horlemann AL, Ramaswamy S, et al. Morphological diversity strongly constrains synaptic connectivity and plasticity. *Cereb Cortex* 2017; 27: 4570–4585.
48. Li Q, Han X, Lan X, et al. Inhibition of neuronal ferroptosis protects hemorrhagic brain. *JCI Insight* 2017; 2: e90777.
49. Zille M, Karuppagounder SS, Chen Y, et al. Neuronal death after hemorrhagic stroke in vitro and in vivo shares features of ferroptosis and necroptosis. *Stroke* 2017; 48: 1033–1043.